Next Materials 7 (2025) 100454

Contents lists available at ScienceDirect

Next Materials

journal homepage: www.sciencedirect.com/journal/next-materials

Research article

Late transition metal complexes bearing chitosan-2,6-pyridine dicarbamide as an intrinsic heterogeneous catalytic converter of 4-nitrophenol

Lateefah Olanike Adebayo [a], Samuel Adeolu Olugbemi [a], Anike Adebayo [a], Olubunmi Kolawole Akiode [b], Moriam Dasola Adeoye [c], Onome Ejeromedoghene [d], Sheriff Adewuyi [a,*]

[a] Department of Chemistry, Federal University of Agriculture Abeokuta, PMB 2240, Abeokuta, Ogun 110001, Nigeria
[b] Department of Chemistry, Nigerian Army University, Biu, PMB 1500, Biu, Borno, Nigeria
[c] Department of Chemical Sciences, Fountain University, PMB 4491, Osogbo, Osun, Nigeria
[d] College of Chemistry, Chemical Engineering and Materials Science, Soochow University, Suzhou, Jiangsu 215123, PR China

ARTICLE INFO

Keywords:
2, 6-pyridinedicarbonyldichloride
Chitosan
4-nitrophenol
Heterogeneous catalyst
Catalytic efficiency
Rate constant

ABSTRACT

The quest for biopolymeric-based heterogeneous catalysts is rapidly increasing owing to added intrinsic recompense. In this study, Chitosan-2, 6-pyridine dicarbamide (CPDC) ligand, and its metal ion complexes [M-CPDC] were synthesized by direct combination method. The characterization of the complexes by FTIR suggested that the amide coordinated with the metal ion through the carbonyl of the amide group. The SEM micrograph of [M-CPDC] showed discrete particles in contrast to the rough surface of CPDC which suggests coordination. The XRD diffractogram of chitosan, CPDC, and [M-CPDC] revealed semi-crystalline, amorphous, and crystalline respectively. The [M-CPDC] were applied as heterogeneous catalysts for the reduction of toxic organic pollutants, 4-Nitrophenol to an environmentally friendly 4-Aminophenol. The synthesized catalysts lowered the activation energy (E_a) range of 0.84–1.30 kJmol^{-1}. However, [CPDC-Ni] showed the highest activity (E_a = 0.84 kJmol^{-1}). The synthesized catalysts displayed higher catalytic activities (reduction process within 60 s) than previously reported. The catalysts were reusable at least five times in the reduction of 4-Nitrophenol.

1. Introduction

Industrial discharge of effluent into the atmosphere, rivers, and seas is a global environmental problem. The majority of the constituents of these effluents are dangerous chemicals such as heavy metals and non-biodegradable organic pollutants which may have adverse effects on man, plants, and aquatic life [1,2]. 4-Nitrophenol (4NIP) is an example of an organic pollutant that largely exists in the environment owing to its application as raw material in several manufacturing industries such as dyes, pesticides, drugs, paper, insecticides, and fine chemicals, etc. [3] and its high stability and solubility in water [4]. 4NIP is deadly and its acute inhalation or ingestion results in headaches, drowsiness, nausea, and cyanosis. It is a great menace to human health; it endangers the central nervous system, brain, livers, kidneys, and blood [5]. It also affects plants and aquatic life. It is listed among the top priorities hazardous materials by the United States Environmental Protection Agency [6]. Hence, detoxification of this chemical before discharging it becomes expedient.

Several methods have been designed for the detoxification of this chemical compound including photocatalytic degradation [7], microbial catabolism [8], biodegradation [9], and the Fenton process [10]. The above-mentioned approaches often give products that are equally or more toxic than 4NIP. From an environmental and industrial perspective, the chemical reduction of 4NIP to 4-Aminophenol (4AMP) in the presence of sodium borohydride as a reducing agent remained an uncomplicated method for the degradation of 4-NIP [11]. 4AMP which is the product of the reduction process is environmentally friendly, less toxic, and an important raw material in the anti-corrosion, beauty product, and pharmaceutical industry [12]. The reduction process is slow under ordinary conditions but can be accelerated in the presence of a catalyst [13,14].

Over the years, precious metal nanoparticles such as silver [15], gold [16], silver/palladium [17], silver/iron oxide [18], gold/palladium nanoalloy [19], Copper nanowires [20], and bismuth [21] have been

* Corresponding author.
E-mail address: adewuyis@funaab.edu.ng (S. Adewuyi).

https://doi.org/10.1016/j.nxmate.2024.100454
Received 4 July 2024; Received in revised form 4 November 2024; Accepted 9 December 2024
Available online 12 December 2024

established as efficacious catalysts for the 4-NIP reduction. Unfortunately, these metals are costly, their separation and recovery are also difficult due to the homogeneous nature of the catalyst. In addition, the environmental impacts of nanoparticles cannot be underestimated. Studies have shown that nanoparticles can diffuse into organisms through inhalation and ingestion and translocate within their body to various organs and tissues and it might result in lung inflammation and heart problems [22].

Adsorption of homogeneous catalysts on inorganic or organic supports to form heterogeneous catalysts has helped to get over the challenges associated with their separation, recovery, reusability, and high cost [23]. A heterogeneous catalytic reaction is a phase separation reaction since the catalysts, reactants, and even the products exist in different phases [24]. However, the significance of support in heterogeneous catalysis cannot be overemphasized. It improves the stability and strength of the metallic catalyst [25]. It also increases the surface area of the catalyst. Inorganic supports are often used as supports in heterogeneous catalysis [26]. Biopolymeric supports such as cellulose and chitosan (CTS) had great preference over inorganic supports due to their availability, inexpensive, low toxicity, low immunogenicity, biocompatibility, sustainability and biodegradability nature [27,28]. Interestingly, the reactive functional hydroxyl and amine groups in CTS confer on the biopolymer, a high sorption capacity for several metal ions that can bind by chemical or physical mode [29]. The presence of free amino groups in the chitosan moiety enables a variety of chemical modifications and substitution processes including carboxylation [30], acylation [31], Schiff's base formation [32], and metal chelation [33]. The modification of chitosan improves its thermal, mechanical, and chemical stabilities. It also increases the internal surface area and thereby improves the catalytic activities of the modified chitosan [34].

Chitosan-based late transition metal complexes have been reported as efficient catalysts for several reactions [35]. Late transition metal complexes of CTS have been reported as efficient catalysts in polymerization [36], Knoevenagal reaction [37], oxidation of methanol [38], and hydrogenation of furfuran [39]. Thus, it is irremissible to design an efficient, stable, economical, and environmentally friendly heterogeneous catalyst for the reduction of 4NIP. However, metal complexes of Copper [40], Cobalt [41], and Ni/Co bimetallic [42] from different ligands have been reported as catalysts for the reduction of 4-NIP. The efficiency of metal complexes varied with the type of ligand [43]. To the best of our knowledge, CTS-based complexes are rarely reported as heterogeneous catalysts for 4-NIP reduction. In light of this, this study aimed at the synthesis of chitosan-2, 6-pyridineadorndicarbamide (CPDC) and investigation of the catalytic activities of its cobalt [Co-CPDC], nickel [Ni-CPDC], and copper complexes [Cu-CPDC] for reduction of 4-NIP. The results obtained are herein presented.

2. Experimental

2.1. Materials and instrumentation

Low molecular weight chitosan (CTS) from crab (75 % deacetylated) and 2, 6-pyridine dicarbonyl dichloride (PDC) (97 %) were purchased from Sigma Aldrich (Kyoto, Japan), anhydrous methanol (99.9 %) was purchased from sigma Aldrich (Germany). Glacial acetic acid, sodium hydroxide, cobalt(II) chloride hexahydrate, nickel(II) chloride hexahydrate, copper (II) sulfate pentahydrate, sodium borohydride, and 4-Nitrophenol were of analytical grade procured from Honeywell Research Chemicals (Ibra Hadad Nigeria Limited, Lagos state. The Fourier Transform Infrared spectrophotometer (FTIR) spectra of the CTS, Chitosan-2,6-pyridine dicarbamide (CPDC) and its metal complexes [M-CPDC] where (M = Co^{2+}, Ni^{2+}, and Cu^{2+}) were recorded on an Agilent Technology Cary 630 FTIR (Delhi, India) with 4 cm^{-1} resolution in the range of 4000–400 cm^{-1}. The electronic absorption spectral studies were carried out using Shimadzu UV-1800 Double Beam UV–visible spectrophotometer (Kyoto, Japan) in the range of 200–800 nm. Surface morphology and Energy Dispersive X-ray (EDX) of the synthesized products were studied with the use of a Carl Xeiss EVO LX10 Scanning Electron Microscope (SEM) (Oberkochen, Germany) with an accelerating voltage of 10 kV at liquid N_2 temperature. Powder X-ray Diffraction (PXRD) of the Chitosan, CPDC, and [M-CPDC] diffractograms were obtained using ADX 2700 Angstrom Advanced X-ray diffractometer (Stoughton, USA) for phase identification.

2.2. Synthesis of chitosan-2, 6-pyridine carbamide and its metal complexes

CTS acylation was performed according to previous literature methods with slight alteration [44]. Practically, CTS (2.2 mmol) was added to 50 mL of 1 % acetic acid solution under magnetic stirring. The pH of the CTS solution was adjusted to 7.00–7.02 with 0.5 M NaOH. PDC (1.1 mmol) was further added to the CTS solution and the resulting product was stirred for 5 h when the color changed from milky gelatinous to brown color. The product obtained was washed with methanol, cast into a petri dish, and air-dried for 24 h and a brown-colored film product was obtained (Scheme 1). Product yield was 86 %.

[Co-CPDC], [Ni-CPDC], and [Cu-CPDC] were synthesized by dissolving CPDC (0.5 mmol) in 1 % acetic acid with continuous stirring at room temperature to ensure complete solubility. The stoichiometric amount of $CoCl_2$, $NiCl_2.6H_2O$, and $CuSO_4.5H_2O$ respectively (0.5 mmol) was dissolved in methanol and added dropwise to the CPDC solution. The reaction was refluxed for 4 h to form a viscous solution. The products were rinsed with methanol to remove unreacted metallic salt and thereafter freeze-dried to obtain the solid products (Scheme 2). The observed color and percentage yields of the products [M-CPDC] after freeze drying are M = Cu^{2+}, (Green, 85 %), Ni^{2+} (Light Green, 77 %), and Co^{2+} (Purple, 78 %).

2.3. Evaluation of catalytic activities of [CPDC-M] complexes

The catalytic activities of [M-CPDC] complexes for 4-NIP reduction using sodium borohydride ($NaBH_4$) as a reducing agent were evaluated. At the start, freshly prepared $NaBH_4$ solution (0.5 mL) was added to the aqueous solution of 4-NIP which changed from light yellow to deep yellow. Thereafter, [Cu-CPDC] (5 mg) was added as a heterogeneous catalyst to the reaction medium, after which the solution turned colorless. A spectrophotometer was set between the wavelength of 200 nm

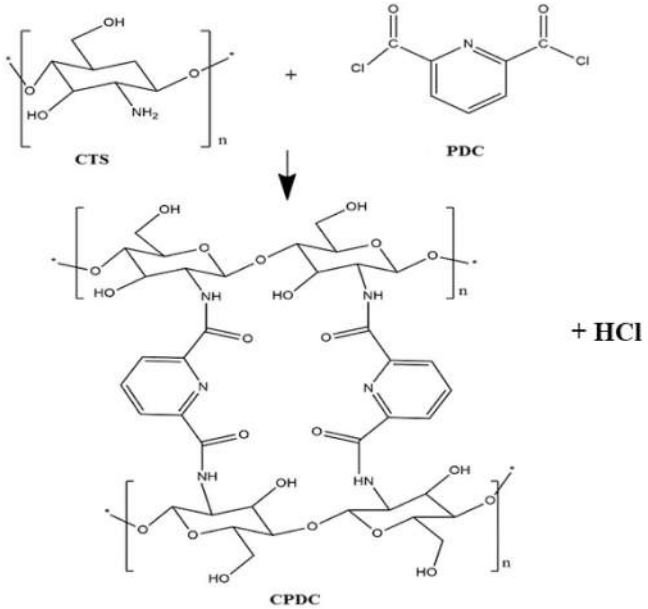

Scheme 1. Synthesis of chitosan-2,6-pyridinedicarbamide (CPDC).

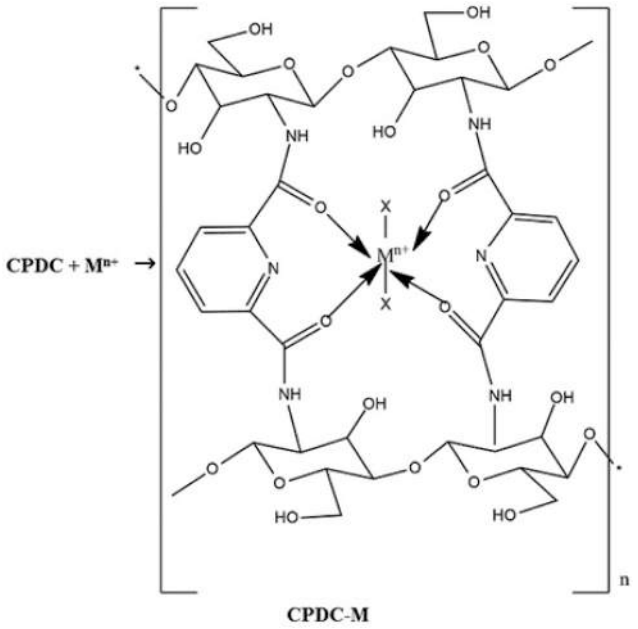

Scheme 2. Synthesis of chitosan-2,6-pyridine dicarbamide metal complexes [M-CPDC] (M = Cu^{2+}, Ni^{2+} and Co^{2+}).

and 600 nm to monitor the progress of the reduction at room temperature. The reduction process was repeated using [Co-CPDC] and [Ni-CPDC] as catalysts.

3. Results and discussions

3.1. UV–visible analysis

The UV-Visible spectra of CPDC and [M-CPDC] complexes are shown in Fig. 1. It has previously been established that chitosan does give rise to UV–Vis absorption due to the absence of chromophoric species in its skeletal framework, thus no peak is expected in the range of 300–800 nm [36,38]. The UV-Visible spectrum of CPDC shows absorption bands at 270 and 329 nm which could be assigned to $\pi \rightarrow \pi^*$ transition of (C═C) available in the pyridine ring and (C═O) $n \rightarrow \pi^*$ transitions respectively [44]. However, these absorption bands differ in wavelength and intensities in the [M-CPDC] spectra. The spectrum of [Ni-CPDC] showed a hypsochromic shift around 315 nm which can be attributed to the interaction between the metal ion and CPDC. Moreover, the spectra of [Cu-CPDC] and [Co-CPDC] show 340 and 350 nm transition bands at a longer wavelength (red shift). These intra-ligand charge transfers (ILCT) and ligand-to-metal charge transfer (LMCT) transitions could plausibly be due to the coordination of amide oxygen to the metal ions [26].

3.2. Infra-red (FTIR) analysis of CPDC and its metal complexes

The FTIR analysis was used to show the functional group present in the prepared compounds and their interactions (Fig. 2). Typically, the infra-red spectrum of chitosan shows a broad peak at 3400 – 3500 cm^{-1} which could be due to the overlapping stretching of OH/NH bond which appears through the link of chitosan with PDC. The peak is observed in chitosan and stretched in CPDC, Co-CPDC, and Ni-CPDC when the ligand donates electrons to the central atom while disappearing in Cu-CPDC due to back donation resulting from saturation of electrons in the *d*-orbital of Cu [45]. It also revealed the bands at 1655, 1589, and 1375 cm^{-1} often assigned to the stretching vibration of amide I, II, and

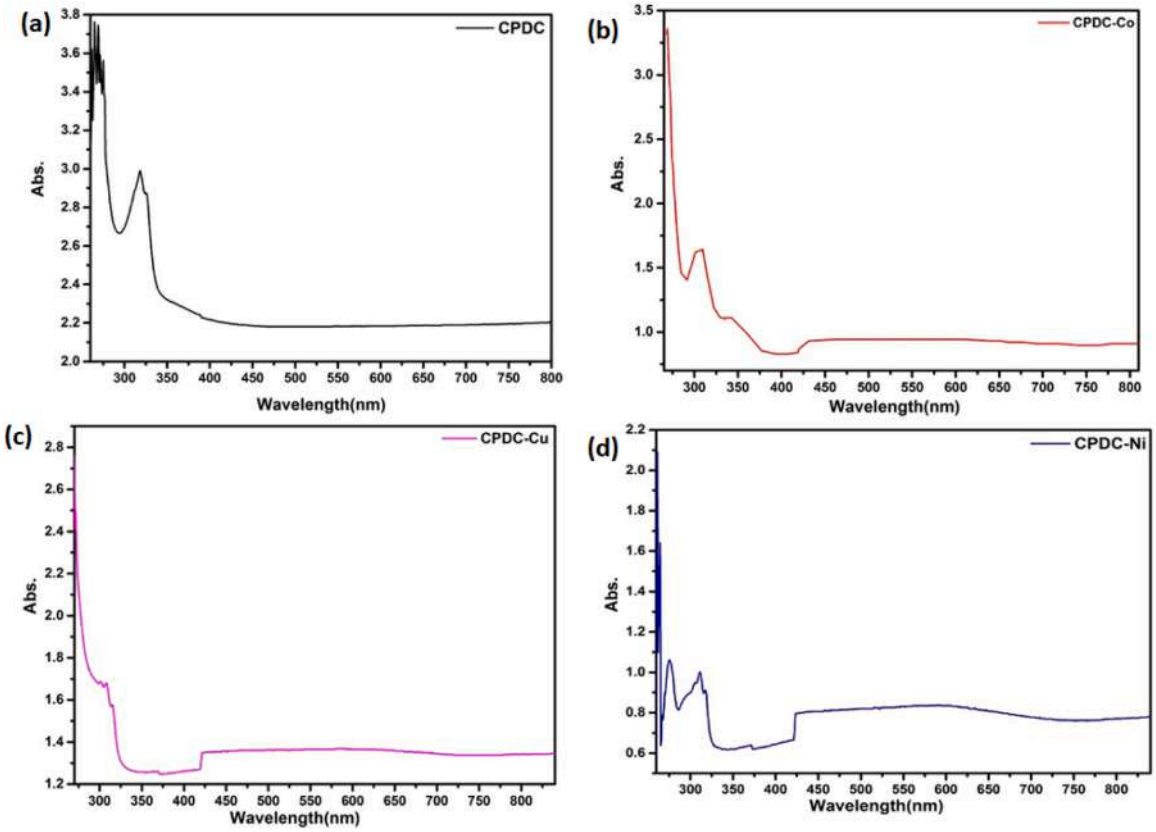

Fig. 1. UV-Vis. spectra of (a) CPDC (b) [Co-CPDC] (c) [Ni-CPDC] and (d) [Cu-CPDC] complexes.

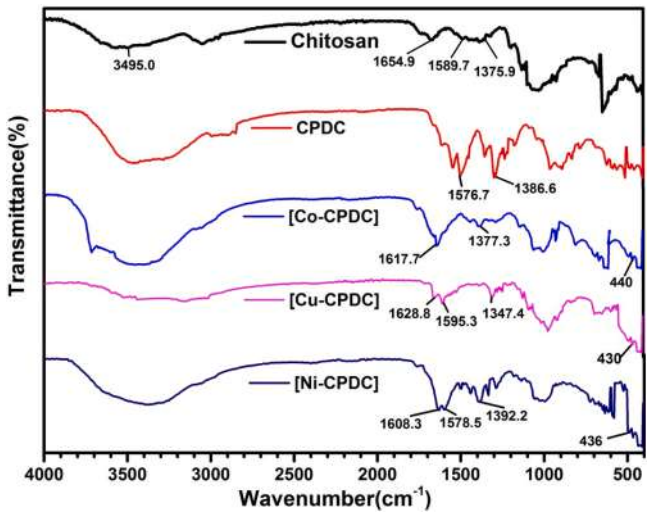

Fig. 2. FTIR spectra of CPDC and its metal complexes.

III ν (C═O, N-H, and C-N) respectively [46]. Expectedly, in the acylated product, these bands shifted to 1678, 1576, and 1387 cm^{-1}, suggesting a new bond formation [47]. However, it is worthy of note that if the biopolymer were fully acylated, the assigned ν(N-H) band would disappear completely [48]. Furthermore, the vibrational frequencies assigned to ν(C═O) bond stretch shifted in the complexes to 1618, 1608, and 1629 cm^{-1} for [Co-CPDC], [Ni-CPDC], and [Cu-CPDC] respectively. This observation is quite suggestive of the coordination of the metal ions with the carbonyl group which is known to be a strong π-donor. Also, new bands were observed in all the metal complexes around 400–500 cm^{-1} assigned to ν(M-O) stretch, further suggesting complex formation [49].

3.3. Powder X-ray diffraction (PXRD)

The crystallinity of the biohybrid ligand as well as the complexes was characterized with PXRD (Fig. 3). Initially, chitosan displayed a characteristic peak at $2\theta = 20.38°$, which suggests its semi-crystalline nature as previously reported [50]. However, the diffractogram of (CPDC) displayed a series of weak peaks which are much wider and weaker than that of chitosan with 2θ and hkl values respectively at 20.85° (111), 23.96° (201), 27.68° (104), 29.45° (203), and 30.37° (210). These correspond to the formation of chaoite with a hexagonal crystal facet according to the Joint Committee on Powder Diffraction Standards (JCPDS) card No. 22–1069.

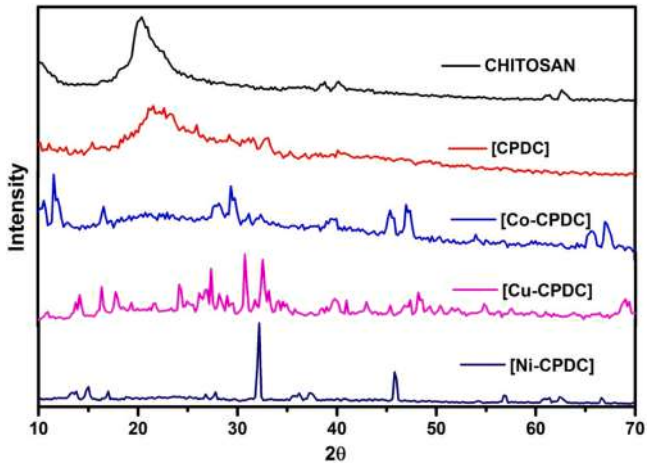

Fig. 3. X-Ray Diffratogram of Chitosan, CPDC, and [M-CPDC].

Furthermore, upon complexation, different series of peaks with varying intensities were obtained with sharp crystalline patterns, which differ considerably from that of the CPDC, portending the coordination of the metal ions with the functional units along the polymer chain [51]. For instance, [Co-CPDC], displayed very weak peaks giving rise to 2θ and hkl values of 19.00° (111), 31.27° (220), 44.80° (400), 49.08° (331), 65.23° (440), and 68.23° (531) respectively, corresponding to the cubic crystal of cobalt oxide according to JCPDS card No. 43–1003. Similarly, [Cu-CPDC] revealed multiple peaks with 2θ= 11.94°, 14.71°, 17.49°, 20.29°, 24.11°, 28.04°, 31.69°, 32.58°, 39.30°, 40.37°, 42.88°, 45.31°, 47.63°, 50.38°, 51.47°, 52.07°, 54.58°, 57.84°, 69.03°, and 69.18° corresponding to (110), (020), (120), (210), (130), (001), (20−1), (21−1), (221), (32−1), (231), (41−1), (350), (43−1), (401), (411), (450), (540), (232), and (081) hkl values. These values corresponded well with the monoclinic crystals of malachite ($Cu_2(OH)_2(CO_3)$) with JCPDS card No. 99–0074. Moreover, 2θ peaks and hkl values respectively captured at 27.59° (101), 31.93° (002), 56.78° (202), and 66.76° (004) were obtained for [Ni-CPDC] and corresponded with Nickel oxide hexagonal crystals of JCPDS card No. 14–0481.

3.4. Scanning electron microscopy (SEM)

The surface morphology of CPDC, [Co-CPDC], [Ni-CPDC], and [Cu-CPDC] complexes were characterized using SEM as displayed in Fig. 4a–d. The different micrographs gave a clear perception of the morphological interaction between the biohybrid ligand and the transition metals. Previously, the SEM micrograph of pure chitosan showed a smooth surface with some straps validating a high degree of chitin deacetylation [52]. Conversely, CPDC showed a fiber-like surface. However, the micrographs of the complexes showed different morphologies of rough surfaces. [Co-CPDC] displayed a rough surface with heterogeneous particles. In addition, [Ni-CPDC] revealed a coarse surface with different size ranges of the block materials, while that of [Cu-CPDC] revealed an aggregated heterogeneous particulate surface. These significant morphological changes also established that there is a coordination of the metal ions with the CPDC ligand. The demonstration of rough surfaces by the complexes gave support to the heterogeneous catalytic capabilities of these complexes.

3.5. Energy–dispersive X-ray spectroscopy (EDX) of the samples

The EDX spectra of CPDC, [Co-CPDC], [Ni-CPDC], and [Cu-CPDC] complexes are displayed in Fig. 5a–d. The EDX spectrum of CPDC showed the presence of carbon, nitrogen, and oxygen peaks which correspond to the elemental constituents of the ligand. Aside from the carbon, nitrogen, and oxygen peaks which were displayed on all the EDX spectra of the metal complexes, Co, Ni, and Cu peaks were also observed in their respective spectra. The appearance of some peaks of some elements such as sulfur and chlorine might be due to the nature of the metallic salts used for complexation.

3.6. Heterogeneous catalytic reduction of 4-nitrophenol to 4-aminophenol

The catalytic performance of [M-CPDC] complexes was investigated through the reduction of 4-nitrophenol to 4-aminophenol as a model system with $NaBH_4$ as a reducing agent. Noticeably, 4-nitrophenol with an initial light-yellow color was observed to show a peak around 320 nm [53,54]. When $NaBH_4$ solution was added, a deep yellow color was observed with peak intensity shifted to 400 nm indicating the formation of 4-nitrophenolate ions as illustrated in Fig. 6a. It was observed that the reduction of nitrophenolate ions at 400 nm was unaffected when the process was left for 2 h in the absence of catalyst. When the new polymeric complexes [M-CPDC] were introduced as a heterogeneous catalyst into the reacting medium, the peak intensity at 400 nm decreased gradually and a new peak intensity at 300 nm was also observed with

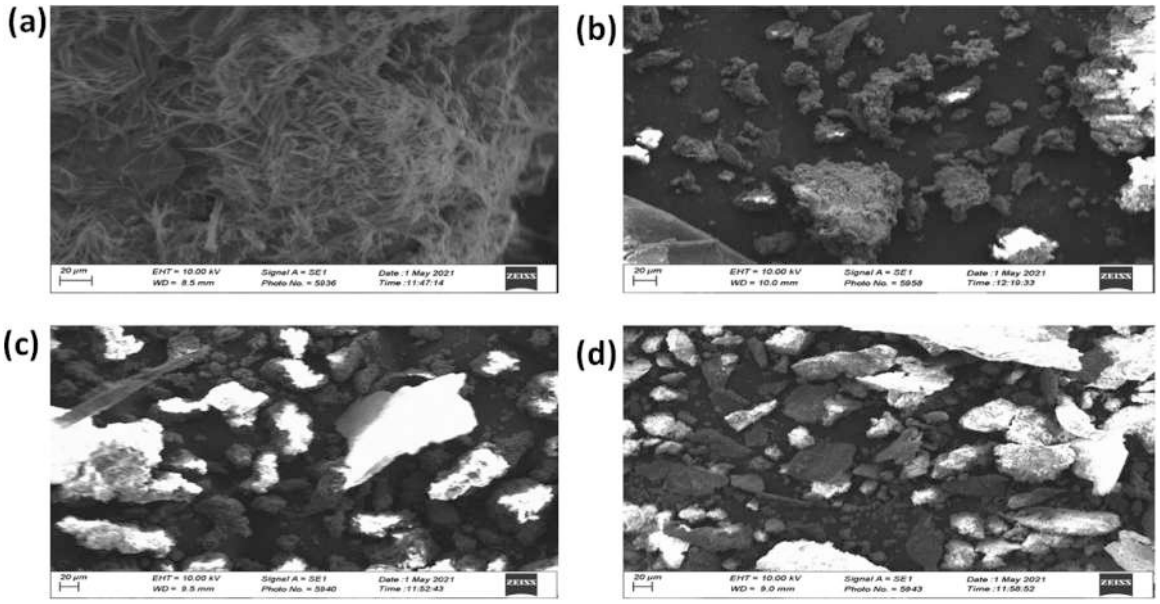

Fig. 4. SEM micrographs of (a) CPDC (b) [Co-CPDC] (c) [Ni-CPDC] and (d) [Cu-CPDC] complexes.

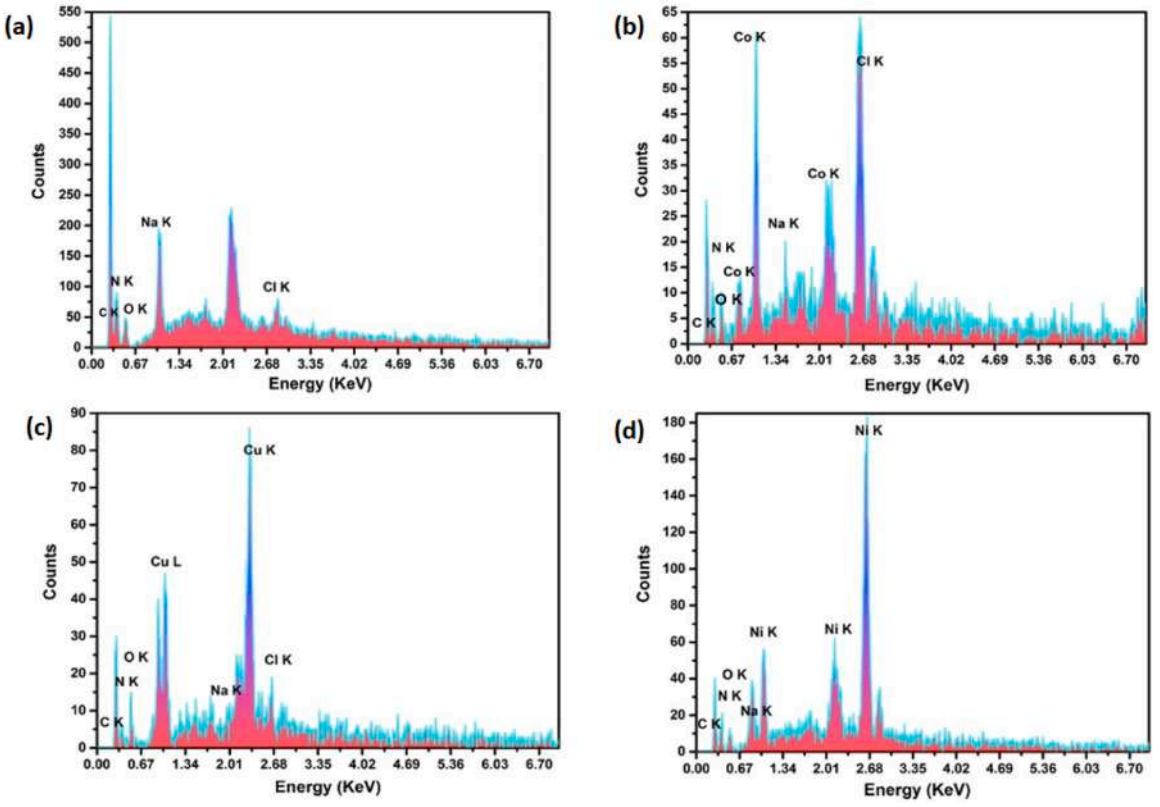

Fig. 5. EDX spectra of (a) CPDC (b) [Co-CPDC] (c) [Ni-CPDC] and (d) [Cu-CPDC] complexes.

time in Fig. 6b. This observation signifies the formation of 4-aminophenol as explained in a previous study [55].

3.7. Kinetic analysis of 4-nitrophenol reduction

The heterogeneous catalytic reduction of 4-nitrophenol to 4-aminophenol was analyzed kinetically by evaluating the effect of different reaction conditions on the reduction process. The effect of contact time, concentration of reactants (4-nitrophenol and $NaBH_4$), and temperature were among the factors evaluated. In each of the analyses, a pseudo-first-order rate constant (k) was proposed because the concentration of $NaBH_4$ was much higher in the reaction than that of 4-nitrophenol [56]. The rate constant was calculated from the slope of the pseudo-first-order equation expressed in Eq. 1.

$$\ln\left(\frac{A_t}{A_O}\right) = \quad -kt \tag{1}$$

The kinetics of the catalytic reduction of 4-nitrophenol to 4-

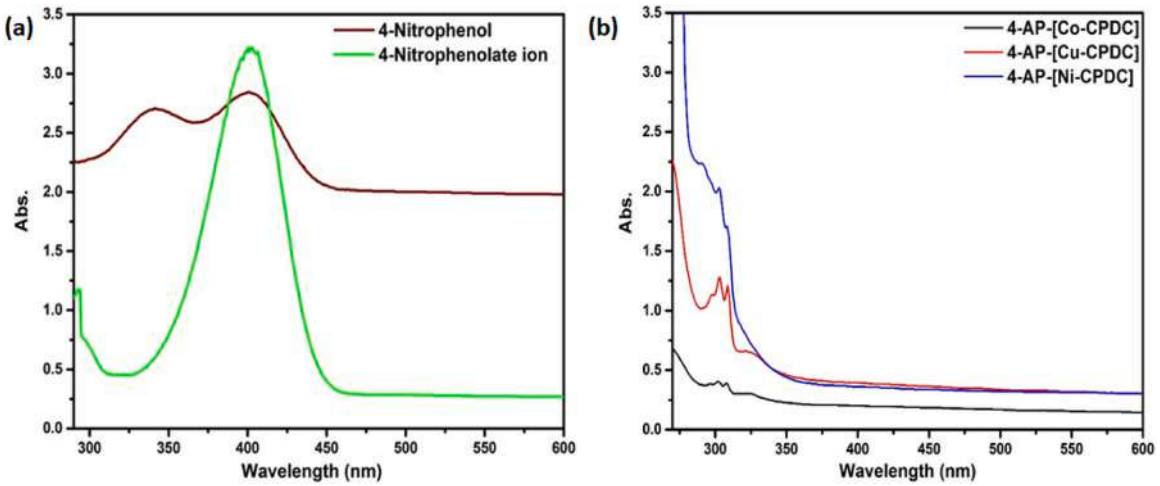

Fig. 6. (a) UV-visible spectra of 4-nitrophenol and 4-nitrophenolate ion (b) UV-visible spectra showing reduction of 4NIP in the presence of [M-CPDC].

aminophenol in the presence of [M-CPDC] were investigated when $\ln A_t/A_0$ against Time (s) were plotted and the value of rate constant (k) and activity constant (A) were deduced. The rate constants obtained were 0.0172 s^{-1}, 0.0165 s^{-1}, and 0.0127 s^{-1} respectively for [Ni-CPDC], [Cu-CPDC], and [Co-CPDC]. For comparison purposes, the activity constants were calculated and the results obtained (Table 1) showed that [Ni-CPDC] had the highest activity (11.4667 $s^{-1}g^{-1}$) followed by [Cu-CPDC] (11.0000 $s^{-1}g^{-1}$) and [Co-CPDC] had the least activity (7.7333 $s^{-1}g^{-1}$). The activity constants of the new catalysts were compared with the literature as shown in Table 1, the results showed that these new systems had higher activity constants than those reported in the literature.

3.7.1. Monitoring of reaction progress at time intervals

The reaction progress was monitored at times of 0, 60, 120, 180, and 240 s using [Ni-CPDC], [Cu-CPDC], and [Co-CPDC] as catalysts. The gradual decrease in intensity of the 400 nm peak was observed in the spectra until time taken for the total disappearance of the peak while a new peak was observed around 300 nm showing the formation of 4-aminophenol [59]. As illustrated in Fig. 7a–c, the observed time for the disappearance of the peak of 400 nm of 4-Nitrophenolate were 120, 60, and 90 s respectively in the presence of [Ni-CPDC], [Cu-CPDC] and [Co-CPDC] as a catalyst. The peak at 400 nm gave no change in the intensity even with a further increase in reaction time in the absence of the catalysts [55,57]. The observed changes in the UV absorption spectra during the catalytic process could be due to the effect of the $NaBH_4$ used in the reaction which can affect the reactions at surfaces by competing with reactants and products for adsorption sites and solvating the adsorbed species [60].

Table 1
Comparison of rate constant (k) and activity constant (A) of [CPDC-M] catalyst systems with reported catalysts for 4-Nitrophenol reduction.

Catalysts	Rate constant (k) (s^{-1})	Activity constant (A) ($s^{-1}g^{-1}$)	Ref.
[Co-CPDC]	0.0116	7.7333	This work
[Cu-CPDC]	0.0165	11.000	This work
[Ni-CPDC]	0.0172	11.467	This work
Au@[C_4C_{16}Im]Br	0.00011	0.0055	[16]
Au/AC nanocatalyst	0.0042	-	[57]
Cu-BDC	0.0151	0.302	[40]
CuO@C	0.006	0.120	[40]
Cu_xO@C−400	0.0048	2.4	[55]
Cu/C porous composite	0.0267	119	[58]
Pt@Ag NP	0.0056	5.6	[6]
Au-Ag bimetallic NPs	0.010		[4]
[Cu_2(TDPH)$_4$(QNX)]	0.0084		[35]

3.7.2. Effect of reactant concentration

The effect of the concentration of reactants on the catalytic reduction process was investigated for clearer insight into the activity of the new catalytic systems. Pseudo-first-order kinetic model was adopted for the evaluation of the rate constant of the catalytic reaction [61] wherein, the concentration of $NaBH_4$ is higher than the concentration of 4-nitrophenol. Fig. 8a–c showed the plots of $\ln(A_t/A_0)$ versus time (sec.) with different concentrations of 4-nitrophenol using 1 M $NaBH_4$ in the presence of [Co-CPDC] [Cu-CPDC] and [Ni-CPDC] respectively.

The effect of varying concentrations of $NaBH_4$ in the reduction reactions was also displayed in Fig. 9a–c by evaluating the plot of $\ln(A_t/A_0)$ versus Time (sec.) with different concentrations of $NaBH_4$ using 1.5 mM 4-nitrophenol in the presence of [Co-CPDC], [Cu-CPDC] and [Ni-CPDC] respectively. The rate constant (k) increases with an increase in the concentration of $NaBH_4$. However, the rate constant decreases with an increase in the concentration of 4-nitrophenol. This is unexpected since increasing reactant concentration usually makes the reaction occur more rapidly. The unexpected phenomenon can be explained by the reaction mechanism. This is due to the higher adsorption affinity for 4-NIP by the catalyst compared to borohydride ions (BH_4^-) giving rise to fewer adsorption sites for BH_4^-.

3.7.3. Effect of temperature and determination of activation energy

Temperature-dependent reduction reactions of 4-nitrophenol to 4-aminophenol were investigated in the presence of [Co-CPDC], [Cu-CPDC], and [Ni-CPDC] as catalysts. The plots of $\ln(A_t/A_0)$ versus Time (sec.) at different temperatures were evaluated and the graph is displayed in Fig. 10a–c. The reduction process increases with an increase in temperature in tandem with the established order. The activation energy for the catalytic reduction was obtained from the slope of the linear plot of $\ln k$ against $1/T$ as shown in Fig. 9 by using the Arrhenius equation.

The activation energy is one of the parameters that show the efficiency of the catalyst by lowering the activation energy of the reaction. The activation energy of the reaction is calculated for each of the reaction. These results were in the order of 0.8422 $kJmol^{-1}$, 0.9595 $kJmol^{-1}$ and 1.1353 $kJmol^{-1}$ for [Ni-CPDC], [Cu-CPDC] and [Co-CPDC] respectively. Consequently, [Ni-CPDC] had the highest catalytic efficiency and [Co-CPDC] had the least efficiency towards reduction of 4-Nitrophenol. Incredibly, these calculated activation energies were much lower than most recently reported catalytic systems (99.4 [33]

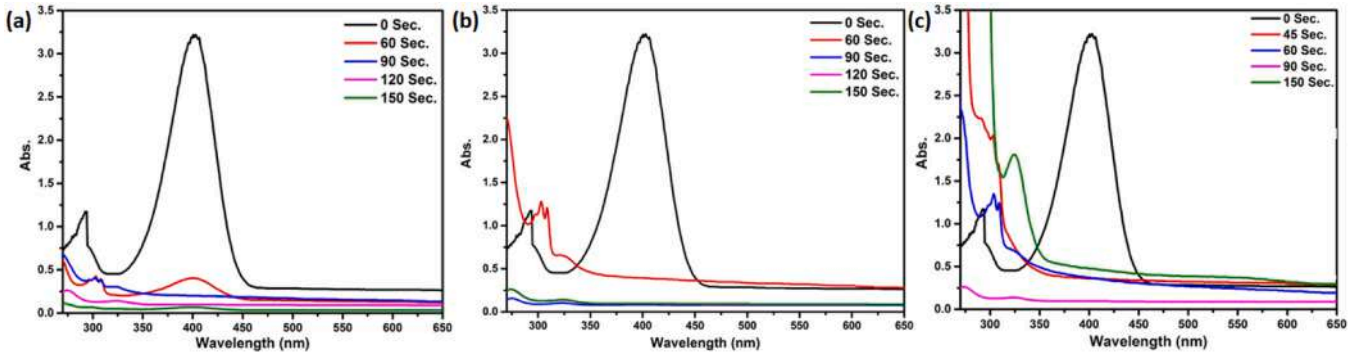

Fig. 7. Time-dependent UV-Visible absorption spectra for the reduction of 4-Nitrophenol with (a) [Co-CPDC] (b) [Cu-CPDC] (c) [Ni-CPDC].

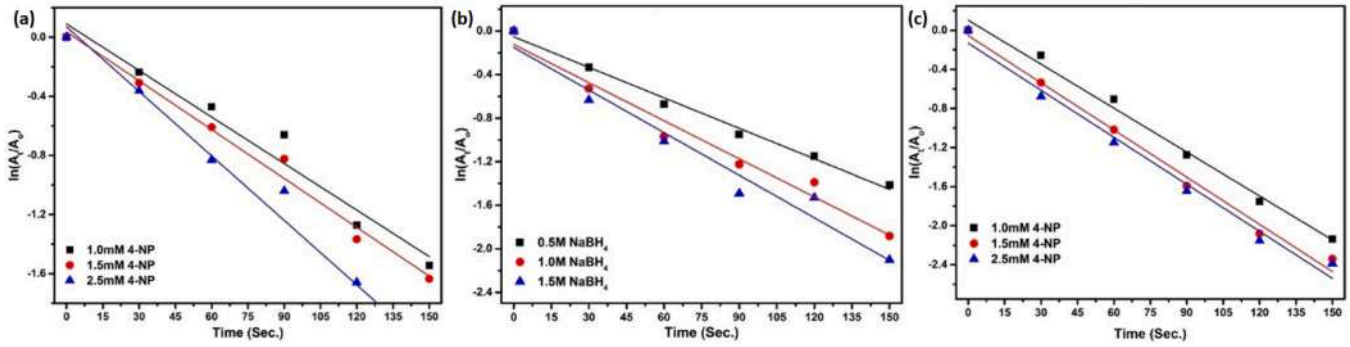

Fig. 8. Effects of 4-NIP concentrations with time using (a) [Co-CPDC] (b) [Cu-CPDC] (c) [Ni-CPDC).

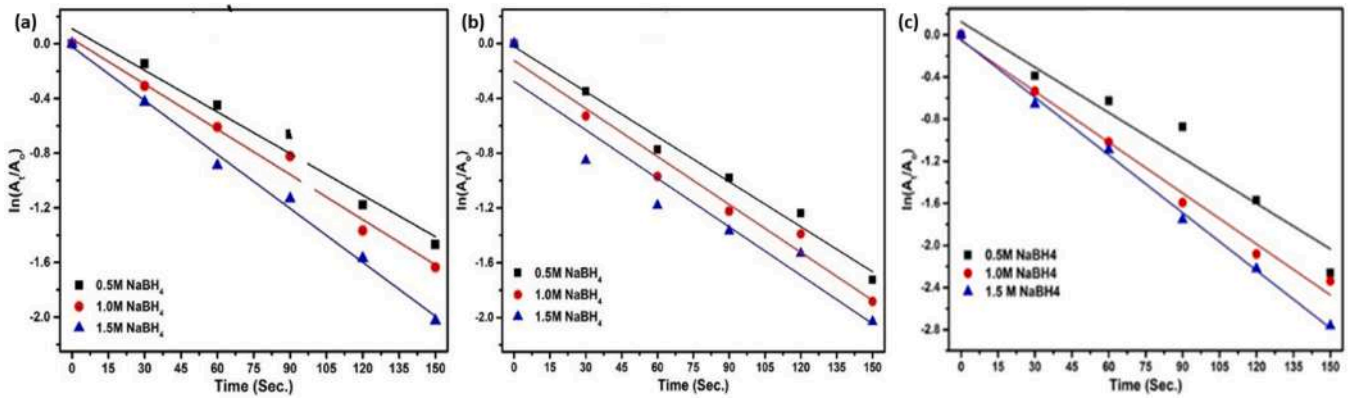

Fig. 9. Effects of $NaBH_4$ concentrations with time using (a) [Co-CPDC] (b) [Cu-CPDC] (c) [Ni-CPDC] as catalysts respectively.

and 26.38 kJmol^{-1} [57]). In effect, these new systems were more efficient than the majority of the recently reported catalysts (Table 2).

The thermodynamic parameters such as enthalpy change (ΔH), free energy change (ΔG), and entropy change (ΔS) were determined from the Erying equation (Eq. 2).

$$\ln k \Big/ T = \ln \frac{k_a}{T} + \frac{\Delta S}{R} - \frac{\Delta H}{R}\left(\frac{1}{T}\right) \quad (2)$$

Where k_a is a Boltzman Constant

But, $\Delta G = \Delta H - T\Delta S$

The thermodynamics parameters are achieved by plotting $\ln k/T$ *against* $1/T$(SI.4) where the slope is $-\Delta H/R$ and the intercept is $\ln k_a/T + \Delta S/R$ [62].

3.8. *Reusability studies of the catalysts*

The reusability studies of [M-CPDC] catalysts were carried out based on the time taken to complete the reaction. Each of these catalysts (M= Co, Ni, Cu) were recycled by centrifugation and decantation. After separation from the reaction medium, the catalysts were washed with distilled water and methanol respectively. Then, the recovered catalysts were air-dried and reused repeatedly five times for the reduction processes. The results obtained are displayed in Fig. 10d. It was observed that there was no significant change in the catalyst activities within five cycles. This observation further confirms the stability of the polymeric metal complexes. However, the little difference might be attributed to particle loss during the decantation process for re-use processes.

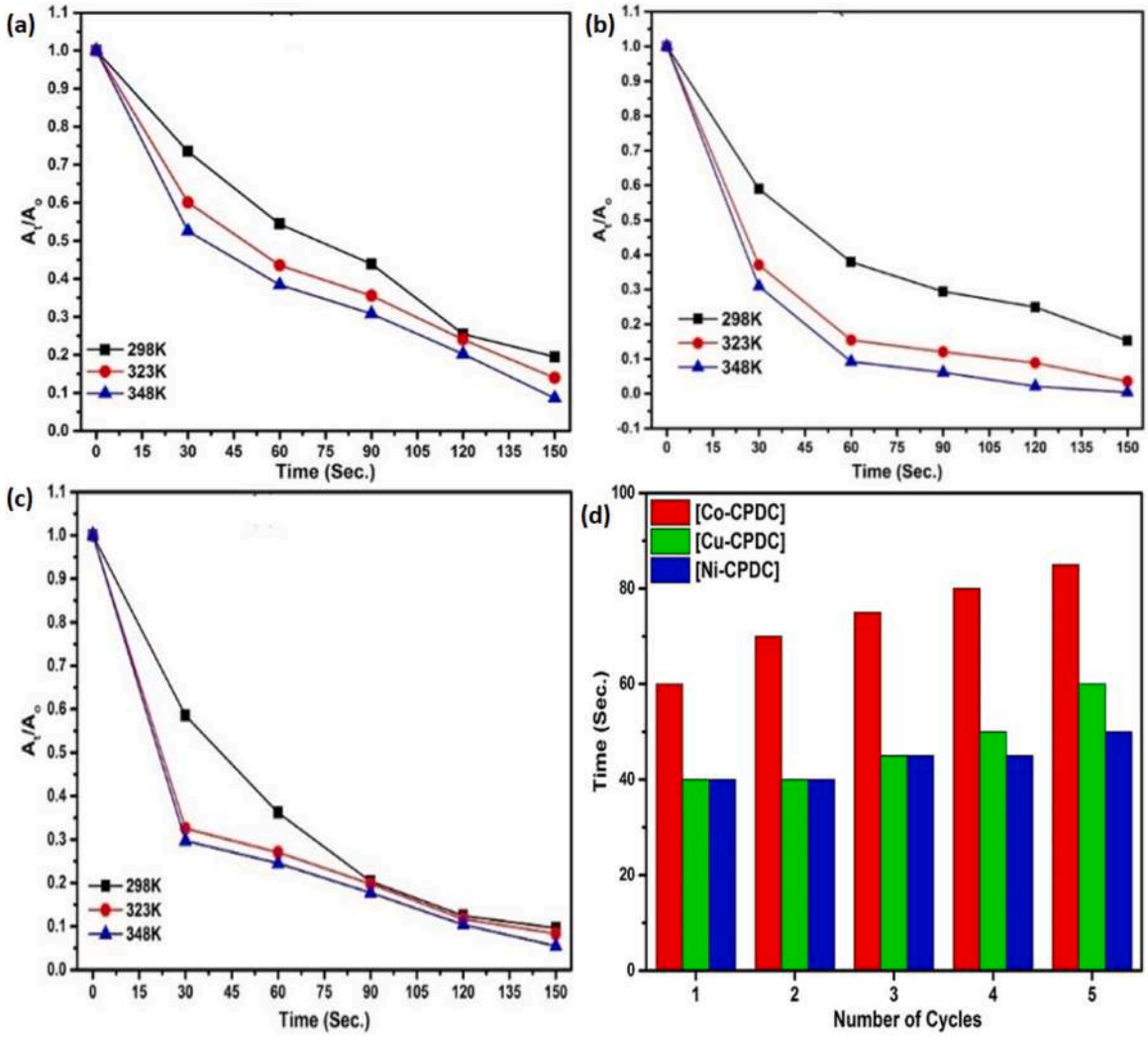

Fig. 10. Effects of reaction temperature with time using (a) [Co-CPDC] (b) [Cu-CPDC] (c) [Ni-CPDC] as a catalyst (d) Reusability studies of [M-CPDC-M] catalytic systems.

Table 2
Comparison of Activation Energy (E_a) and Enthalpy of reaction (ΔH) of synthesized catalysts with reported catalysts for 4-Nitrophenol reduction.

Catalysts	Activation Energy (E_a) ($kJmol^{-1}$)	Enthalpy of reaction (ΔH) ($kJmol^{-1}$)	References
[Co-CPDC]	1.0821	1.4633	This work
[Cu-CPDC]	0.9595	1.3674	This work
[Ni-CPDC]	0.8422	1.6646	This work
Au@[C_4C_{16}Im]Br	99.4000	96.8500	[16]
Au/AC nanocatalyst	26.38	32.14	[57]

4. Conclusion

This study depicts excellent functionalization of chitosan biopolymer with coordination extending 2,6-pyridinedicarbonyl dichloride ligand and corresponding metal ion complexes formation. These new systems functioned appropriately in the heterogeneous catalytic conversion of 4-nitrophenol to 4-aminophenol via the reduction process of $NaBH_4$. These new bio-inspired metal complexes were compared with the previously reported systems at the nanometric scale in terms of catalytic reactivity. The synergic effect of the coordination extension afforded by the cross-linking ligand promoted the active metal centers for catalytic conversion. With very low activation energies and conversion time, these complexes acted as efficient heterogeneous catalyst systems.

Declaration of Competing Interest

The authors declare that they have no known competing financial interests or personal relationships that could have appeared to influence the work reported in this paper.

Acknowledgements

This work was supported by the Department of Chemistry, Federal University of Agriculture, Abeokuta, Nigeria. L.O. Adebayo acknowledges Engr—S. A. Fadare for the financial aid.

References

[1] L. He, D.D. Liu, B.B. Wang, H.B. Xu, Removal of heavy metals from aqueous solution by poly(ethyleneimine)-functionalized silica: studies on equilibrium isotherm, kinetics, and thermodynamics of interactions, Res. Chem. Intermed. 41 (2015) 3913–3928, https://doi.org/10.1007/s11164-013-1499-z.
[2] K.H. Hama Aziz, F.S. Mustafa, K.M. Omer, S. Hama, R.F. Hamarawf, K.O. Rahman, Heavy metal pollution in the aquatic environment: efficient and low-cost removal approaches to eliminate their toxicity: a review, RSC Adv. 13 (2023) 17595–17610, https://doi.org/10.1039/d3ra00723e.

[3] A. Serrà, R. Artal, M. Pozo, J. Garcia-Amorós, E. Gómez, Simple environmentally-friendly reduction of 4-nitrophenol, Catalysts 10 (2020) 1–12, https://doi.org/10.3390/catal10040458.

[4] N. Berahim, W.J. Basirun, B.F. Leo, M.R. Johan, Synthesis of bimetallic gold-silver (Au-Ag) nanoparticles for the catalytic reduction of 4-nitrophenol to 4-aminophenol, Catalysts 8 (2018) 1–15, https://doi.org/10.3390/catal8100412.

[5] N.K.R. Bogireddy, A.G. El Hachimi, Y.R. Mejia, M.K. Kesarla, R.S. Varma, R. H. Becerra, V. Agarwal, Pyridinic N anchored Ag and Au hybrids for detoxification of organic pollutants, npj Clean Water 40 (2022) 1–13, https://doi.org/10.1038/s41545-022-00187-w.

[6] Z.S. Lv, X.Y. Zhu, H.Bin Meng, J.J. Feng, A.J. Wang, One-pot synthesis of highly branched Pt@Ag core-shell nanoparticles as a recyclable catalyst with dramatically boosting the catalytic performance for 4-nitrophenol reduction, J. Colloid Interface Sci. 538 (2019) 349–356, https://doi.org/10.1016/j.jcis.2018.11.109.

[7] Z. Abbasi, E.I. García-López, G. Marcì, A. Farrokhnia, M.Z. Shoushtari, Photocatalytic degradation of 4-Nitrophenol by g-C3N4-MCy: mechanism study and kinetic modeling, J. Photochem. Photobiol. A Chem. 407 (2021) 113004, https://doi.org/10.1016/j.jphotochem.2020.113004.

[8] J. Min, L. Xu, S. Fang, W. Chen, X. Hu, Molecular and biochemical characterization of 2-chloro-4-nitrophenol degradation via the 1,2,4-benzenetriol pathway in a Gram-negative bacterium, Appl. Microbiol. Biotechnol. 103 (2019) 7741–7750, https://doi.org/10.1007/s00253-019-09994-7.

[9] D. Kalaimurugan, P. Sivasankar, K. Durairaj, M. Lakshmanamoorthy, S. Ali Alharbi, S.A. Al Yousef, A. Chinnathambi, S. Venkatesan, Novel strategy for biodegradation of 4-nitrophenol by the immobilized cells of Pseudomonas sp. YPS3 with Acacia gum, Saudi J. Biol. Sci. 28 (2021) 833–839, https://doi.org/10.1016/j.sjbs.2020.11.019.

[10] V.N. Lima, C.S.D. Rodrigues, Y.B. Brandão, M. Benachour, L.M. Madeira, Optimisation of the degradation of 4-nitrophenol by Fenton's process, J. Water Process Eng. 47 (2022) 102685, https://doi.org/10.1016/j.jwpe.2022.102685.

[11] M. Ruan, P. Song, J. Liu, E. Li, W. Xu, Highly efficient regeneration of deactivated Au/C catalyst for 4-nitrophenol reduction, J. Phys. Chem. C 121 (2017) 25882–25887, https://doi.org/10.1021/acs.jpcc.7b08787.

[12] M. Najafi, S. Azizian, Catalytic reduction of 4-nitrophenol on the surface of copper/copper oxide nanoparticles: a kinetics study, Appl. Nanosci. 10 (2020) 3827–3837, https://doi.org/10.1007/s13204-020-01485-w.

[13] Y. Qin, J. Luo, Y. Zhao, C. Yao, Y. Li, Q. An, Z. Xiao, S. Zhai, Dual-wastes derived biochar with tailored surface features for highly efficient p-nitrophenol adsorption, J. Clean. Prod. 353 (2022) 131571, https://doi.org/10.1016/j.jclepro.2022.131571.

[14] C. Gao, Q. An, Z. Xiao, S. Zhai, B. Zhai, Z. Shi, Alginate and polyethyleneimine dually mediated synthesis of nanosilver-containing composites for efficient p-nitrophenol reduction, Carbohydr. Polym. 181 (2018) 744–751, https://doi.org/10.1016/j.carbpol.2017.11.083.

[15] M. Mourya, D. Choudhary, A.K. Basak, C.S.P. Tripathi, D. Guin, Ag-nanoparticles-embedded filter paper: an efficient dip catalyst for aromatic nitrophenol reduction, intramolecular cascade reaction, and methyl orange degradation, ChemistrySelect 3 (2018) 2882–2887, https://doi.org/10.1002/slct.201702609.

[16] S.R. Thawarkar, B. Thombare, B.S. Munde, N.D. Khupse, Kinetic investigation for the catalytic reduction of nitrophenol using ionic liquid stabilized gold nanoparticles, RSC Adv. 8 (2018) 38384–38390, https://doi.org/10.1039/c8ra07404f.

[17] X.Y. Zhu, Z.S. Lv, J.J. Feng, P.X. Yuan, L. Zhang, J.R. Chen, A.J. Wang, Controlled fabrication of well-dispersed AgPd nanoclusters supported on reduced graphene oxide with highly enhanced catalytic properties towards 4-nitrophenol reduction, J. Colloid Interface Sci. 516 (2018) 355–363, https://doi.org/10.1016/j.jcis.2018.01.047.

[18] J.R. Chiou, B.H. Lai, K.C. Hsu, D.H. Chen, One-pot green synthesis of silver/iron oxide composite nanoparticles for 4-nitrophenol reduction, J. Hazard. Mater. 248–249 (2013) 394–400, https://doi.org/10.1016/j.jhazmat.2013.01.030.

[19] S. Gu, Y. Lu, J. Kaiser, M. Albrecht, M. Ballauff, Kinetic analysis of the reduction of 4-nitrophenol catalyzed by Au/Pd nanoalloys immobilized in spherical polyelectrolyte brushes, Phys. Chem. Chem. Phys. 17 (2015) 28137–28143, https://doi.org/10.1039/c5cp00519a.

[20] A.S. Hashimi, M.A.N.M. Nohan, S.X. Chin, S. Zakaria, C.H. Chia, Rapid catalytic reduction of 4-nitrophenol and clock reaction of methylene blue using copper nanowires, Nanomaterials 9 (2019) 1–13, https://doi.org/10.3390/nano9070936.

[21] Y.A. Alli, S. Adewuyi, B.S. Bada, S. Thomas, H. Anuar, Quaternary trimethyl chitosan chloride capped bismuth nanoparticles with positive surface charges: catalytic and antibacterial activities, J. Clust. Sci. 33 (2022) 2311–2324, https://doi.org/10.1007/s10876-021-02156-8.

[22] I. Khan, K. Saeed, I. Khan, Nanoparticles: properties, applications and toxicities, Arab. J. Chem. 12 (2019) 908–931, https://doi.org/10.1016/j.arabjc.2017.05.011.

[23] M. Nasrollahzadeh, N. Motahharifar, Z. Nezafat, M. Shokouhimehr, Copper(II) complex anchored on magnetic chitosan functionalized trichlorotriazine: an efficient heterogeneous catalyst for the synthesis of tetrazole derivatives, Colloids Interface Sci. Commun. 44 (2021) 100471, https://doi.org/10.1016/j.colcom.2021.100471.

[24] M.E. Ali, M.M. Rahman, S.M. Sarkar, S.B.A. Hamid, Heterogeneous metal catalysts for oxidation reactions, J. Nanomater. 2014 (2014) 1–23, https://doi.org/10.1155/2014/192038.

[25] R. Kumar, P. Wang, W. Xue, Y. Jia, Z. Zhu, L. Luo, J.W.-C. Wong, J. Zhao, Catalytic oxidation of 5-hydroxymethylfurfural to 2,5-furandicarboxylic acid using Co-N/C catalysts with stepwise base addition approach, Next Mater. 5 (2024) 100227, https://doi.org/10.1016/j.nxmate.2024.100227.

[26] S. Anuradha, D.D. Kumari, Pathak, Synthesis and development of chitosan anchored copper(II) Schiff base complexes as heterogeneous catalysts for N-arylation of amines, Tetrahedron Lett. 56 (2015) 4135–4142, https://doi.org/10.1016/j.tetlet.2015.05.049.

[27] A. Al-Azmi, S. Keshipour, Cross-linked chitosan aerogel modified with Pd(II)/phthalocyanine: synthesis, characterization, and catalytic application, Sci. Rep. 9 (2019) 1–10, https://doi.org/10.1038/s41598-019-50021-6.

[28] S.A. Olugbemi, L.O. Adebayo, S. Adewuyi, A new Pyrrole-2-carboxaldehyde functionalized chitosan-Cu(II) complex-based chemosensor for iodide anion in aqueous media, Chem. Sci. Int. J. 32 (2023) 1–12, https://doi.org/10.9734/csji/2023/v32i5855.

[29] M.A. Al-Issa, A.A. Abbas, F.S. Matty, Synthesis and characterization of Schiff base derived from chitosan and its complexes With (Co+2, Ni+2 and Cu+2), Ibn AL-Haitham, J. Pure Appl. Sci. 29 (2017) 115–129. ⟨https://jih.uobaghdad.edu.iq/index.php/j/article/view/90⟩.

[30] T. Jin, D. Kurdyla, S. Hrapovic, A.C.W. Leung, S. Régnier, Y. Liu, A. Moores, E. Lam, Carboxylated chitosan nanocrystals: a synthetic route and application as superior support for gold-catalyzed reactions, Biomacromolecules 21 (2020) 2236–2245, https://doi.org/10.1021/acs.biomac.0c00201.

[31] E.M. de A. Braz, S.C.C.C. e. Silva, D.A. da Silva, F.A. de A. Carvalho, H.M. Barreto, L. de S. Santos Júnior, E.C. da Silva Filho, Modified chitosan-based bioactive material for antimicrobial application: synthesis and characterization, Int. J. Biol. Macromol. 117 (2018) 640–647, https://doi.org/10.1016/j.ijbiomac.2018.05.205.

[32] S. Khare, N. Tiwari, Catalytic study of highly recoverable chitosan supported Cu(II) Schiff base complex for alkanes oxidation, React. Kinet. Mech. Catal. 136 (2023) 3053–3077, https://doi.org/10.1007/s11144-023-02501-0.

[33] S. Adewuyi, N.O. Sanyaolu, S.A. Amolegbe, A.O. Sobola, O.M. Folarin, Poly [β-(1→4)-2-amino-2-deoxy-D-ghicopyranose] based zero valent nickel nanocomposite for efficient reduction of nitrate in water, J. Environ. Sci. 24 (2012) 1702–1708, https://doi.org/10.1016/S1001-0742(11)60903-0.

[34] S. Le Grill, Y. Coppel, J. Soulie, G. Bertrand, C. Rey, F. Brouillet, Towards chitosan-amorphous calcium phosphate nanocomposite: Co-precipitation induced by spray drying, Next Mater. 4 (2024) 100095, https://doi.org/10.1016/j.nxmate.2023.100095.

[35] A.C. Tella, S.O. Owalude, V.O. Adimula, A.C. Oladipo, V.T. Olayemi, B. Ismail, A. Mumtaz, A.U. Rehman, A.M. Khan, H.S. Clayton, N.M. Tahir, Synthesis, structure, and properties of a dinuclear Cu(II) coordination polymer based on Quinoxaline and 3,3-Thiodipropionic acid ligands, J. Inorg. Organomet. Polym. Mater. 31 (2021) 3089–3100, https://doi.org/10.1007/s10904-021-01966-7.

[36] S. Adewuyi, I.O. Bisiriyu, C.A. Akinremi, S.A. Amolegbe, Synthesis, spectroscopic, surface and catalytic reactivity of chitosan supported Co(II) and its zerovalentcobalt nanobiocomposite, J. Inorg. Organomet. Polym. Mater. 27 (2017) 114–121, https://doi.org/10.1007/s10904-016-0452-1.

[37] R. Mary, A. Xavier, N. Romeo, Synthesis, characterization and catalytic applications of chitosan based Schiff base complexes of copper (II), Int. J. Res. Appl. Sci. Eng. Technol. 10 (2022) 511–516, https://doi.org/10.22214/ijraset.2022.47037.

[38] A.O. Adebayo, E.O. Ogunbiyi, L.O. Adebayo, S. Adewuyi, Schiff base modified chitosan iron(III) complex as new heterogeneous oxidative catalyst, J. Chem. Soc. Niger. 46 (2021) 289–295.

[39] A. Guerrero-Torres, C.P. Jiménez-Gómez, J.A. Cecilia, J.M. Porras-Vázquez, C. García-Sancho, J.J. Quirante-Sánchez, F. Guerrero-Ruíz, R. Moreno-Tost, P. Maireles-Torres, Synthesis of catalysts by pyrolysis of Cu-chitosan complexes and their evaluation in the hydrogenation of furfural to value-added products, Mol. Catal. 512 (2021) 111774, https://doi.org/10.1016/j.mcat.2021.111774.

[40] A.A. Kassem, H.N. Abdelhamid, D.M. Fouad, S.A. Ibrahim, Catalytic reduction of 4-nitrophenol using copper terephthalate frameworks and CuO@C composite, J. Environ. Chem. Eng. 9 (2021) 104401, https://doi.org/10.1016/j.jece.2020.104401.

[41] X. Zhang, F. Jin, A cobalt(II) coordination polymer based on a carboxyl- triazolyl-bifunctional ligand: synthesis, characterization and catalytic reduction of 4-nitrophenol, Inorg. Chem. Commun. 119 (2020) 108075, https://doi.org/10.1016/j.inoche.2020.108075.

[42] V.O. Adimula, A.C. Tella, S.O. Owalude, A.C. Oladipo, V.T. Olayemi, E. Adeniyi, B. Ismail, A. Mumtaz, A.M. Khan, Synthesis, characterization and catalytic studies of bimetallic heteronuclear complexes for the reduction of nitroaromatic compounds, Inorg. Nano-Met. Chem. 53 (2023) 501–512, https://doi.org/10.1080/24701556.2022.2078364.

[43] H.W. Garba, M.S. Abdullahi, M.S.S. Jamil, N.A. Endot, Efficient catalytic reduction of 4-nitrophenol using copper(Ii) complexes with n,o-chelating schiff base ligands, Molecules 26 (2021) 1–12, https://doi.org/10.3390/molecules26195876.

[44] P. Abrica-González, J.A. Zamora-Justo, A. Sotelo-López, G.R. Vázquez-Martínez, J. A. Balderas-López, A. Muñoz-Diosdado, M. Ibáñez-Hernández, Gold nanoparticles with chitosan, N-acylated chitosan, and chitosan oligosaccharide as DNA carriers, Nanoscale Res. Lett. 14 (2019) 1–14, https://doi.org/10.1186/s11671-019-3083-y.

[45] G.M. Su, H. Wang, B.R. Barnett, J.R. Long, D. Prendergast, W.S. Drisdell, Backbonding contributions to small molecule chemisorption in a metal-organic framework with open copper(i) centers, Chem. Sci. 12 (2021) 2156–2164, https://doi.org/10.1039/d0sc06038k.

[46] S.R. Bhattarai, R. Bahadur K.C, S. Aryal, M.S. Khil, H.Y. Kim, N-acylated chitosan stabilized iron oxide nanoparticles as a novel nano-matrix and ceramic modification, Carbohydr. Polym. 69 (2007) 467–477, https://doi.org/10.1016/j.carbpol.2007.01.006.

[47] J. Wang, Y. Zhou, Y. Shao, F. He, M. Wu, H. Ni, Y. Zheng, Y. Sun, Chitosan–silica nanoparticles catalyst (M@CS–SiO 2) for the degradation of 1,1-

dimethylhydrazine, Res. Chem. Intermed. 45 (2019) 1721–1735, https://doi.org/10.1007/s11164-018-3697-1.
[48] R. Shelma, C.P. Sharma, Acyl modified chitosan derivatives for oral delivery of insulin and curcumin, J. Mater. Sci. Mater. Med. 21 (2010) 2133–2140, https://doi.org/10.1007/s10856-010-4073-x.
[49] A.A.A. Emara, M.A. Tawab, M.A. El-Ghamry, M.Z. Elsabee, Metal uptake by chitosan derivatives and structure studies of the polymer metal complexes, Carbohydr. Polym. 83 (2011) 192–202, https://doi.org/10.1016/j.carbpol.2010.07.040.
[50] O. Ejeromedoghene, O. Oderinde, X. Ma, M. Olusola, S. Adewuyi, G. Fu, Reroute green synthesis of hexagonal and triclinic nanostructured cerium oxide: morphology and optical properties, J. Mater. Sci. Mater. Electron. (2021), https://doi.org/10.1007/s10854-021-06183-z.
[51] A.S. Montaser, A.R. Wassel, O.N. Al-Shaye'a, Synthesis, characterization and antimicrobial activity of Schiff bases from chitosan and salicylaldehyde/TiO2 nanocomposite membrane, Int. J. Biol. Macromol. 124 (2019) 802–809, https://doi.org/10.1016/j.ijbiomac.2018.11.229.
[52] C.S. Thatte, M.V. Rathnam, A.C. Pise, Chitosan-based Schiff base-metal complexes (Mn, Cu, Co) as heterogeneous, new catalysts for the β-isophorone oxidation, J. Chem. Sci. 126 (2014) 727–737, https://doi.org/10.1007/s12039-014-0601-4.
[53] N. Yılmaz Baran, Palladium nanoparticles decorated on a novel polyazomethine as a highly productive and recyclable catalyst for Suzuki coupling reactions and 4-nitrophenol reduction, J. Organomet. Chem. 899 (2019) 120886, https://doi.org/10.1016/j.jorganchem.2019.120886.
[54] S. Liu, A. Qileng, J. Huang, Q. Gao, Y. Liu, Polydopamine as a bridge to decorate monodisperse gold nanoparticles on Fe3O4 nanoclusters for the catalytic reduction of 4-nitrophenol, RSC Adv. 7 (2017) 45545–45551, https://doi.org/10.1039/c7ra09373j.
[55] L. Zhi, H. Liu, Y. Xu, D. Hu, X. Yao, J. Liu, Pyrolysis of metal-organic framework (CuBTC) decorated filter paper as a low-cost and highly active catalyst for the reduction of 4-nitrophenol, Dalton Trans. 47 (2018) 15458–15464, https://doi.org/10.1039/C8DT03327G.
[56] K. Dhanapal, S. Dhanavel, T.A. Revathy, V. Narayanan, A. Stephen, Catalytic behavior of magnetic Ni–Zn alloy, Res. Chem. Intermed. 44 (2018) 4149–4161, https://doi.org/10.1007/s11164-018-3360-x.
[57] A. Kumar, M. Belwal, R.R. Maurya, V. Mohan, V. Vishwanathan, Heterogeneous catalytic reduction of anthropogenic pollutant, 4-nitrophenol by Au/AC nanocatalysts, Mater. Sci. Energy Technol. 2 (2019) 526–531, https://doi.org/10.1016/j.mset.2019.05.007.
[58] Y. Bai, Q. Wang, C. Du, T. Bu, Y. Liu, X. Sun, W. Luo, R. Li, Y. Zhao, X. Zheng, L. Wang, Three-dimensional Cu/C porous composite: facile fabrication and efficient catalytic reduction of 4-nitrophenol, J. Colloid Interface Sci. 553 (2019) 768–777, https://doi.org/10.1016/j.jcis.2019.06.079.
[59] K. Hasan, I.A. Shehadi, N.D. Al-bab, A. Elgamouz, Magnetic chitosan-supported silver nanoparticles, Catalysts 9 (2019) 839.
[60] C. Sievers, S.L. Scott, Y. Noda, L. Qi, E.M. Albuquerque, R.M. Rioux, Phenomena affecting catalytic reactions at solid−Liquid interfaces, ACS Catal. 6 (2016) 8286–8307, https://doi.org/10.1021/acscatal.6b02532.
[61] F. Xia, X. Xu, X. Li, L. Zhang, L. Zhang, H. Qiu, W. Wang, Y. Liu, J. Gao, Preparation of bismuth nanoparticles in aqueous solution and its catalytic performance for the reduction of 4-nitrophenol, Ind. Eng. Chem. Res. 53 (2014) 10576–10582, https://doi.org/10.1021/ie501142a.
[62] P. Guo, L. Tang, J. Tang, G. Zeng, B. Huang, H. Dong, Y. Zhang, Y. Zhou, Y. Deng, L. Ma, S. Tan, Catalytic reduction-adsorption for removal of p-nitrophenol and its conversion p-aminophenol from water by gold nanoparticles supported on oxidized mesoporous carbon, J. Colloid Interface Sci. 469 (2016) 78–85, https://doi.org/10.1016/j.jcis.2016.01.063.